https://doi.org/10.5194/acp-2022-555
Preprint. Discussion started: 19 September 2022

Atmospheric Chemistry and Physics Discussions

Satellite (GOSAT-2 CAI-2) retrieval and surface (ARFINET) observations of Aerosol Black Carbon over India

Mukunda M. Gogoi[1], S. Suresh Babu[1], Ryoichi Imasu[2], Makiko Hashimoto[3]

[1]Space Physics Laboratory, Vikram Sarabhai Space Centre, ISRO, Thiruvananthapuram 695-022, India
[2]Atmosphere and Ocean Research Institute, The University of Tokyo, Chiba 277-8568, Japan
[3]Space Technology Directorate I, Earth observation research centre, JAXA, Ibaraki 305-8505, Japan

Correspondence to: Mukunda M. Gogoi (mukunda.mg@gmail.com), Ryoichi Imasu (imasu@aori.u-tokyo.ac.jp)

Abstract. The light-absorbing Black Carbon (BC) aerosols have very sensitive role in affecting the Earth's radiation budget and climate. In this study, satellite-based retrieval of BC over India is presented based on observations from the Cloud and Aerosol-Imager-2 (CAI-2) on-board the Greenhouse gases Observing Satellite-2 (GOSAT-2). To evaluate and validate the satellite retrievals, near surface BC mass concentrations measured across a network of aerosol observatories (ARFINET) over India are used and the findings are extended to comprehend the global BC features. As the analysis revealed, this satellite retrieval fairly depicts the regional and seasonal features of BC over the Indian region, which are similar to those recorded by surface observations. The validation and closure studies between the two data sets show RMSE < 1 and absolute difference below 2 μg m^{-3} for > 60% of simultaneous observations, possessing fairly good associations in Dec-Jan-Feb (R ~ 0.73) and Mar-Apr-May (R ~ 0.76). Over the hotspot regions of India, the satellite retrievals show soot volume fraction of ~ 5%, columnar single scattering albedo of ~ 0.8 and BC column optical depth of ~ 0.1; which are comparable to that of other in-situ or satellite measurements. In terms of global spatio-temporal variability, satellite retrieval shows higher BC occurring mostly in areas where biomass burning is intense. Overall, this study highlights the effectiveness of satellite retrieval of BC, which could be effectively used for the regular monitoring of BC load arising out of vehicular/ industrial/ biomass burning activities across the globe.

1 Introduction

The convergence of various experimental and modeling studies on the climate warming potential of atmospheric Black Carbon (BC) necessitates its accurate quantification and seasonal source characterization at the regional and global scale (Bond et al., 2013; Gustaffson and Ramanathan, 2016; IPCC, 2021). Concerted efforts have been made to understand the radiative properties (warming as well as offsetting the scattering effects of aerosols) of BC arising out of the incomplete combustion of bio-fuel or fossil-fuel sources. Though nearly accurate estimation of BC is made using in-situ approach (uncertainty in BC measurements < 5-10%; Manoj et al., 2019), most of the studies confining to in-situ measurements (ground based or air-borne) have limited spatial coverage. Similarly, model simulated BC though have good spatio-temporal coverage are subjected to deviations from the real BC environment, mainly due to the inaccurate model inventories and meteorological input available for the simulations (Vignati et al., 2010). In this regard, retrieval of BC from satellite-based radiation measurements synchronizing with the ground-based point-measurements is a novel idea to quantify and classify the real BC environment across distinct geographic regions of the globe. However, the very challenging task is to accurately retrieve backscattering signal from optically thin BC aerosols lofted above highly heterogeneous land surfaces, such as vegetated, desert, semiarid and urban regions, having diverse surface reflectance properties. The complex optical properties of BC arising out of the highly heterogeneous sources and transformation processes add further complexity to the satellite retrieval, especially over the land. Even though several new algorithms have been developed for aerosol retrieval over land (e.g., Multi-Angle Imaging Spectroradiometer (MISR) retrieval by Dinner et al., 1998; Dark Target method by Levy et al., 2007; Multi-Angle Implementation of Atmospheric Correction (MAIAC) by Lyapustin et al., 2011; Deep Blue method by Hsu et al., 2013; UV

https://doi.org/10.5194/acp-2022-555
Preprint. Discussion started: 19 September 2022

Atmospheric Chemistry and Physics Discussions

method by Fukuda et al., 2013; Multi-Angle and Polarization Measurements of Radiations by Dubovik et al., 2011, 2014; Multi-Wavelength and -Pixel Method (MWPM) by Hashimoto and Nakajima, 2017), the direct retrieval of BC from satellite based radiation measurement have not addressed so far.

The objective of this paper is to present the regional distribution of BC over India based on satellite-based observations by Cloud and Aerosol-Imager-2 (CAI-2) on-board Greenhouse gases Observing Satellite-2 (GOSAT-2). To evaluate and validate the spatio-temporal distribution of BC from satellite retrieval, near surface BC mass concentrations measured across a network of aerosol observatories over India (ARFINET; Babu et al., 2013; Gogoi et al., 2021) are used and the findings are extended to comprehend the global BC features. The main purpose of CAI-2 is to derive cloud areas to improve accuracy in greenhouse gas (GHG) retrieval by Fourier Transform Spectrometer (FTS) in addition to determining the concentrations of BC mass and fine particulate matter (PM2.5) based on aerosol optical thickness of fine mode particles. CAI-2 is a push-broom imaging sensor which records the backscattered radiances at 7-wavelengths/ 10-sepctral bands in UV (339, 377 nm), VIS (441, 546, 672 nm) and NIR (865, 1630 nm) equipped in forward (339, 441, 672, 865 and 1630 nm) and backward (377, 546, 672, 865 and 1630 nm) looking directions (± 20°). GOSAT-2 makes 89 laps for observing the whole globe in 6 days (swath ~ 920 km). Starting from the ascending node, each satellite revolution data is defined as a CAI-2 scene. Each of the scene is divided in to 36 equal parts (each part is called as frame) by the argument of latitude at observation point of central pixel. A file unit of CAI-2 archives the data of one frame. Since the scene for CAI-2 archives the data of only day side, 18 files are generated from one satellite revolution.

In the ARFINET, the main objective of the measurements of various aerosol parameters (e.g., columnar aerosol optical depth, BC mass concentrations, etc.) is to develop periodic and accurate estimates of aerosol radiative forcing over India and assess their impacts on regional and global climate, taking into account their heterogeneous properties in space, time and spectral domains. Since its very modest beginnings in 1985, the network has expanded to more than 40 observatories today. Supplementary Table-T1 provides more details regarding the ground-based observational locations in the ARFINET. The stations are arranged and grouped with respect their geographic positions in the Indo-Gangetic Plains (IGP); Northeastern India (NEI); Northwestern India (NWI); Himalayan, sub-Himalayan and foothills regions (HIM), Central India (CI), Peninsular India (PI) and Island Locations (IL). The systematic and long-term monitoring of BC in the ARFINET began in 2000, followed by gradual extension of the observational sites in phases. In this study, the use of ground-based BC from the ARFINET is unique in a way that the BC over the Indian region is highly heterogeneous, both in terms of spatial and temporal scales (Manoj et al., 2019; Gogoi et al., 2017; 2021). With rapidly growing industrial and transport sectors, mixed with diverse uses of fossil and bio-fuels in the domestic and industrial sectors, the Indian region is a complex blend of emissions and atmospheric processes (Babu et al., 2013; Gogoi et al., 2021). While the shallow atmospheric boundary layer leads to very high concentrations of BC near the surface in winter (Dec-Feb), especially over the northern part of India (Nair et al., 2007; Pathak et al., 2010; Gogoi et al., 2013, Vaishya et al., 2017 etc.), the synoptic circulations and convective processes are dominant in horizontal and vertical re-distribution of BC in the pre-monsoon (Mar-May) and monsoon (Jun-Sep) seasons (Babu et al., 2016; Nair et al., 2016; Gogoi et al., 2019, 2020). Thus, the synergistic study of the regional BC distribution by combining satellite and surface measurements over the Indian region is unique in terms of enabling retrieval accuracy as well as expanding it to the understanding of global distribution in near-real time.

2 Data and Methodologies

2.1 Retrieval of BC from Cloud and Aerosol Imager -2 (CAI-2)

For cloud discrimination as well as deriving aerosol properties, CAI-2 Level 1B (L1B) radiance data is converted to apparent reflectance, minimum reflectance and surface albedo which are pre-requisites. The apparent reflectance R is calculated as

https://doi.org/10.5194/acp-2022-555
Preprint. Discussion started: 19 September 2022

Atmospheric Chemistry and Physics Discussions

$$R = \frac{\pi L}{\mu_0\left(F_0/_{d^2}\right)} \quad (1)$$

where L is the satellite measured radiance, μ_0 is the cosine of solar zenith angle, F_0 is the solar constant and d is distance between earth and sun (in AU). The new surface reflectance correction algorithm (Fukuda et al., 2013; CAI-2 L2 pre-processing ATBD) uses minimum reflectance data at UV (339 nm in forward viewing band-1 and 377 nm in backward viewing band-6), visible (670 nm in forward viewing bands-3 and backward viewing band-8) and NIR (865 nm in forward viewing band-4 and backward viewing band-9), along with the NDVI to estimate the surface albedo. The first and second minimum reflectance at 670 nm are selected from multiple day from about two-months data between $X_{day} - n1$ and $X_{day} + n2$ day, where X_{day} is an analysis day and n1 and n2 are the number of scenes required before and after the analysis date that take the same path as the analysis date. When the difference between first and second minimum is smaller than a threshold for band-1 (339 nm; forward viewing) and band-6 (377 nm; backward viewing), i.e., $R_{(2nd,min)band1,6} - R_{(1st,min)band1,6} < 0.10$; and greater than a threshold for band-4 (865 nm; forward viewing) and band-9 (865 nm; backward viewing), i.e., $R_{(2nd,min)band4,9} - R_{(1st,min)band4,9} > 0.06$; the first minimum reflectance of the bands 3 and 8 are judged to be affected by cloud shadows and the second minimum reflectance is selected as a minimum reflectance (Fukuda et al., 2013). The advantage of using near-UV wavelengths is that the surface reflectance at UV over land is smaller than that at visible wavelengths, as is already applied for aerosol retrieval in TOMS and OMI (Torres et al., 1998; 2002; 2007; 2013) and the MODIS (Hsu et al., 2004; 2006). Assuming that there is no aerosol in the minimum reflectance data, the surface albedo is derived by performing a correction removing the influence of atmospheric molecular scattering (Rayleigh scattering). For this, radiative transfer calculations are performed in advance and look-up tables (LUT) are generated to correct the influence of atmospheric molecular scattering required for deriving the surface albedo. The LUTs required for correcting the molecular scatterings are generated for atmospheric single scattering and multiple scattering components of reflectance, unidirectional transmittance, and spherical albedo. Following this, surface albedo is derived for different combinations of satellite-solar geometry. For the retrieval of columnar aerosol optical depth (AOD) from the satellite received path radiances, a multiple-wavelength multiple-pixel (MWPM) inversion algorithm developed by Hashimoto and Nakajima (2017) is used. This algorithm utilizes information contained in different pixels with different surface reflectance and it is assumed that aerosol properties vary slowly or are almost negligibly in the horizontal direction where the variation in surface properties are significant. Thus, the changes in the upward radiances over different pixels are assumed to be varying due to variations in surface reflectance at the respective pixels. This is an extension of the method by Kaufman (1987), reporting that for specific surface condition (known as neutral reflectance), the apparent reflectance does not change with aerosol load (AOD) due to the cancellation of increasing atmospheric path radiance and decreasing surface-reflected radiance. As the variation in radiances take place with variation in AOD depending on aerosol light absorption (or single scattering albedo - SSA) and surface reflectance, this principle is suitable for successful retrieval of SSA value over different surface reflectance areas. A zero balance in the change in the upward radiances is obtained when the brightening due to scattering is compensate by the darkening due to absorption. This balance is utilized via a radiative transfer model to derive the SSA. Hashimoto and Nakajima (2017) adapted the same principle, but extending it to multiple wavelength and multiple pixels. The information contained in radiances at each of the pixels with different surface reflectance are used together, rather than solving radiative transfer equation (RTE) for pixel by pixel independently. In addition, the simultaneous use of short and long wavelengths in the CAI-2 bands is very effective for aerosol retrieval when the surface is covered by vegetation and bare soil depending on the location. The flowchart of CAI-2 L2 preprocessing algorithm is shown in the supplementary Figure-S1.

The BC mass concentration (M_{BC}) is derived (CAI-2 L2 aerosol retrieval ATBD) using the size distribution of fine mode particles, the fine mode AOD at 550 nm ($\tau 550_{fine}$), and the volume fraction of BC in fine mode particles (f_{BC}). The expression for M_{BC} can be given as

$$M_{BC} = \frac{1}{m} f_{BC} \rho_{BC} \int_{r_{min}}^{r_{max}} \frac{dV_{fine}(\tau 550_{fine})}{dlnr} dlnr \quad (2)$$

https://doi.org/10.5194/acp-2022-555
Preprint. Discussion started: 19 September 2022

Atmospheric Chemistry and Physics Discussions

Here, ρ_{BC} is density of BC (~ 1.8 g cm^{-3}), V_{fine} is the volume of fine mode particles, r is the radius of particles and m the aerosol height information parameter (~ 1000 m in this study). As M_{BC} is 1000 m averaged values of column fine mode aerosol particle amount in this study, thus the definition is different from BC mass concentrations obtained by in-situ ground-based measurements.

For the estimation f_{BC}, an internal mixture of fine-mode aerosols and soot particles (by soot volume fraction, SF) are considered representative of aerosol light absorption by the fine-mode particles. Thus, $f_{BC} = V_{soot}/V_{fine}$, where V_{soot} is the soot volume in the fine mode. In the beginning, an a-priori value of soot is assumed as 0.1 and the retrieval parameter 'u' is investigated based on it's a-priori state 'u_a'. Several a-priori values around the true-states 'u_t' are considered in the experiment; such as $u_t \pm 0.5u_t$ for $AOT500_{fine}$, $AOT500_{coarse}$, and SF, and $u_t \pm 0.1u_t$ for surface reflectance. The a-priori values of $AOD500_{fine}$ and $AOD500_{coarse}$ are considered as 0.1, 0.2, 0.4 and 0.5. The iteration in the solution search is stopped when the threshold is < 0.01 (Hashimoto and Nakajima, 2017). Several sensitivity studies on this aspect revealed that the retrieval of AOD shows higher uncertainty over the high-reflectance surface, whereas the uncertainty in SF retrieval is higher over the low-reflectance surface. However, the simultaneous retrieval with multiple pixels with different surface reflectance in this study is an effective way to increase the accuracy of aerosol retrieval over diverse land surface properties.

2.2 Surface BC Measurements in the ARFINET

Near surface mass concentrations of BC are obtained from the multi-wavelength aethalometer measurements in the ARFINET. The aethalometers measure the rate of increase in optical absorption due to BC deposit on a filter spot (Hansen et al., 1984). By knowing the change in the optical attenuation by the volume of air (i.e., the mass flow rate multiplied by the sampling time) and the spot area of the filter, the BC concentrations (in μg m^{-3}) can be estimated. The measurement of the rate of change of optical absorption on a single collecting spot can be subject to non-linearity due to the nature and composition of the aerosol (Park et al. 2010), which is prominent in earlier-model Aethalometers (models AE-16, AE-21, AE-22, AE-31, AE-42-2 and AE-42-7) as against the latest model (AE-33). As the spot gradually becomes darker, the calculated output concentration can be under-reported; reverting to the correct value when the tape advances to a fresh spot. Provided that a continuous data record exists, which spans several tape advances due to loaded and fresh tape spots, it is possible to post-process the data. This recalculates the BC data for each wavelength, in addition to providing the value of the filter loading compensation parameter, which is found to be indicative of aerosol properties (Drinovec et al., 2017). In this study, the quality of BC data is ensured following the uniformity of measurements by aethalometers of different models. Regular servicing, calibrations and inter-comparison of the instruments are also made in the ARFINET for quality data collection. Detail about the aethalometer uncertainty and correction of raw-data is available in Gogoi et al., (2017). The overall uncertainty in BC mass measured by the Aethalometer is estimated at about 10%.

2.3 BC Column Optical Depth

Employing the values of soot volume fraction (f_{BC}) as well as mass absorption efficiency of BC with its columnar content, the columnar optical depth due to BC (BC_{AOD}) over the study domain is estimated. Following *Wang et al*., (2013), the expression for optical depth due to BC (BC_{AOD}) can be given as

$$AOD_{BC} = \sigma_{abs}\rho_{BC}V_{BC} \quad (6)$$

where, σ_{abs} is the mass absorption coefficient due to BC, ρ_{BC} is the density of BC (assumed as 1.8 g cm^{-3}), $V_{BC}(= f_{BC}.V_{total})$ is the volume concentrations of BC in the vertical column and V_{total} is total volume concentrations of aerosols in the vertical column. Following Schuster et al., (2005), the volume concentrations of BC can be estimated from the columnar mass concentrations of BC_{col} (in μg m^{-2}, up to 1 km altitude in the present study) as:

https://doi.org/10.5194/acp-2022-555
Preprint. Discussion started: 19 September 2022

Atmospheric Chemistry and Physics Discussions

$$BC_{col} = f_{BC}\rho_{BC}\int \frac{dV}{dlnr} dlnr \quad (7)$$

For estimating σ_{abs} for the columnar content of BC, a constant value of mass absorption efficiency, MAE = 10 m^2 g^{-1} is used. BC mass absorption efficiency (i.e., absorption coefficients of the particles divided by the mass concnetrations of BC in the aerosol) indicates the light absorbing efficiency of certain amount of BC having different mixing and sizes (Martins et al., 1998). Several investigators have reported the MAE of BC varying between 4.3 to 15 m^2g^{-1}, even though the measured values for freshly generated BC fall within a relatively narrow range of 7.5 ± 1.2 m^2g^{-1} at 550 nm (Bond et al., 2013). However, this value can be suitable for measurements close to the source of BC. As the ambient BC in the atmosphere is mostly aged in nature, a value of MAE = 10 m^2g^{-1} is used (Kondo et al., 2009), which is also recommended by the commercial particle soot absorption photometer (PSAP) manufacturer. Sand et al., (2021) have also reported a model mean value of MAC as 10.1 (3.1 to 17.7) m^2 g^{-1} (550 nm).

3 Results and Discussions

3.1 Regional distribution of BC over India

For the distinct geographical regions of India with a variety of emissions and transformation processes of carbonaceous aerosols, the spatiotemporal distributions of BC from satellite (GOSAT-2 CAI-2) retrieval (of the years 2019 and 2020) and surface measurements (climatological data) in the ARFINET are shown in Fig. 1 (for December-January-February, DJF), Fig. 2 (for March-April-May, MAM) and Fig. 3 (June-July-August, JJA), representing three distinct periods of winter, pre-monsoon, and monsoon respectively.

In winter (DJF), the surface observations (Fig. 1) depict the highest BC mass concentrations (M_{BC}) in the IGP (13.67 ± 5.65 µg m^{-3}) followed by NEI (12.35 ± 4.87 µg m^{-3}), with M_{BC} exceeding 7 µg m^{-3} in most locations. A number of polluted locations exhibit values above 15 µg m^{-3}, with the highest values occurring in urban centers. BC concentrations remain lower (< 5.5 µg m^{-3}) over the NWI (~ 4.67 ± 3.48 µg m^{-3}), CI (~ 5.36 ± 0.80 µg m^{-3}) and PI (~ 4.51 ± 3.02 µg m^{-3}) and lowest across the HIM (including sub-Himalayan and foothill sites; average BC ~ 2.26 ± 1.75 µg m^{-3}). Similar to the surface observations, satellite retrievals over the IGP and NEI show higher BC with magnitude comparable to those of the surface BC measurements. Pockets of higher BC are also apparent at some of the locations of PI from both satellite retrievals and surface measurements. It is also consistent with the surface observations that satellite retrieved BC is higher over the eastern coast of India.

Satellite retrievals during pre-monsoon (MAM, Fig. 2) also clearly show regional hotspots of BC over the IGP and NEI as seen in the surface measurements (IGP ~ 7.05 ± 1.78 µg m^{-3} and NEI ~ 4.88 ± 1.13 µg m^{-3}). Both in satellite retrievals and surface measurements, BC remains below 3 µg m^{-3} over the NWI, CI and PI regions. The gradual decline in BC from DJF to MAM is also clearly evident in the satellite retrievals. A rise in temperature caused by increased solar heating during this period, results in strong convection over the Indian region, which in turn leads to dilutions of near-surface aerosol concentrations.

During monsoon (JJA, Fig. 3), the satellite retrievals are not fully congruent with the surface measurements, especially in the CI and PI regions. The average values of surface measured BC over the IGP and NEI are 3.93 ± 1.64 µg m^{-3} and 2.64 ± 1.30 µg m^{-3} respectively, with M_{BC} < 2 µg m^{-3} over the rests of the regions. There is also a gradual decline in magnitude from DJF through MAM to JJA in the surface measurements. As opposed to this, satellite retrievals show higher BC (> 3 µg m^{-3}) in several pockets of CI and PI regions, particularly during July and August with values higher than during MAM. Based on these observations, it appears that satellite retrievals closely match the surface observations of BC over the Indian region during DJF and MAM.

https://doi.org/10.5194/acp-2022-555
Preprint. Discussion started: 19 September 2022

Atmospheric Chemistry and Physics Discussions

Satellite retrievals vs climatological surface BC concentrations

The comparison of the 1 x 1 degree area average BC from satellite retrievals (around each of the observational sites) with the climatological (2015-2019) monthly average surface BC concentrations (obtained during 13:00 to 14:00 hrs. local time) at different months of winter, pre-monsoon and monsoon show the consistency of satellite retrievals (Supplementary Fig. S2; the statistical fit parameters are given in Supplementary Table T2). It is evident that the linear correlation between the two data sets is highest in May (R ~ 0.79). R > 0.6 during February through August. In the months of December and January, R < 0.5. On a seasonal term, the satellite retrievals and surface observations show better associations during MAM (R ~ 0.70). In JJA, the association between the two data sets is weak (R ~ 0.50) and the least in DJF (R ~ 0.43). Thus, despite satellite retrievals during winter and pre-monsoon months showing the regional hotspots of BC over India fairly well, there appears to be a lack of consistent associations between the two datasets in winter at some of the ARFINET observational sites.

The above observations point to the varying role of geographical features, as well as to the heterogeneity of BC abundance and vertical distribution in the atmosphere over different seasons. As the satellite retrieved BC is 1-km column average fine mode particle concentrations, the role of planetary boundary layer (PBL) dynamics and columnar pattern of BC distribution are crucial in understanding the association between satellite and surface measured BC. In locations having PBL height of ~ 1 km is expected to demonstrate better associations between the two than in locations with much extended (h > 1 km) or shallow (h < 1 km) PBL. Thus, the spatio-temporal variability of PBL could be an important factor in explaining the association between satellite retrieval and climatological surface BC measurements.

Despite this, the regional average BC over the entire Indian region (Fig. 4) shows that the satellite retrievals differ from surface measured BC by < 33% in most months, except Jul and Aug (> 50%). In Feb-Aug, the magnitudes of satellite retrieved BC are lower (underestimates, as much as 32.6% in February) compared to surface measurements; while it is opposite (overestimates) in Dec-Jan and Jun-Aug, with highest overestimation in August (~ 69%). Seasonally, the difference between the two data sets over the entire Indian region is < 20% in DJF and MAM and ~ 53.5% in JJA (Table-1). In general, the surface measurements of BC concentrations over the entire Indian region show a gradual decline from its highest values in DJF (2.54 ± 0.11 μg m^{-3}) through MAM (2.06 ± 0.47) to its lowest value in JJA (1.11 ± 0.17 μg m^{-3}). Similar to this, the 1-km column average satellite retrieved BC also show highest BC concentrations over the collocated locations of India during DJF and its gradual decline in MAM. However, the regional average values of the satellited retrieved BC are found to be higher in JJA than in MAM. These observations hint again the discrepancy between satellite retrievals and surface measured BC in JJA, while there is a fair association between the two during DJF and MAM in most locations.

Day-to-day satellite retrievals vs surface BC concentrations

After studying the association between satellite retrieved BC and climatological monthly average surface BC levels in DJF, MAM and JJA, we will now examine simultaneous day-to-day values of BC from the satellite retrievals and surface measurements. Since the satellite retrieved BC corresponds to 1-km column average fine mode particle concentrations, the measured BC concentrations in the surface are normalized to a PBL height of 1 km for utilizing in the validation experiment. For this, it is assumed that BC possesses uniform vertical profile within the well mixed PBL and their concentrations are negligible above the PBL. Thus, the expression relating the 1-km column concentration of BC in the surface ($BC_{SUR\text{-}N}$) and the BC concentrations measured within the PBL (BC_{SUR}) can be given as

$$BC_{SUR\text{-}N} = BC_{SUR} / h \quad (3)$$

Here, h is the height of the PBL layer, and the measured concentrations of BC in the PBL is assumed as the sum of concentrations in each layer of thickness 'dh' from surface to the PBL height h (i.e., $BC_{SUR-N} = \int_0^h BC_i(h)dh$; here, '$i$' is the

https://doi.org/10.5194/acp-2022-555
Preprint. Discussion started: 19 September 2022

Atmospheric Chemistry and Physics Discussions

number of layers from 0 to h). For h = 1, $BC_{SUR\text{-}N} = BC_{SUR}$. The higher the PBL height above 1 km, the greater the measured BC concentration in the surface than that measured within 1 km PBL and vice versa. As the seasonally varying PBL heights at different ARFINET sites might play important role in understanding the association between the satellite retrieval and the surface measured BC, the normalized values of surface BC concentrations ($BC_{SUR\text{-}N}$) are used in this section to evaluate and validate the simultaneous (corresponding to satellite overpass time) day-to-day values of satellite retrieved (1-km column average) BC. The PBL height information is obtained from ERA5. Similar methodology has been reported by Bao et al., (2019).

The frequency distributions of the absolute differences between the two datasets are shown in Fig. 5a, which indicate good agreements between the simultaneous satellite retrieved BC (BC_{SAT}) and surface measured BC ($BC_{SUR\text{-}N}$). Approximately 60% of the satellite retrieved BC is comparable (absolute difference < 2 μg m^{-3}) to surface measurements in all three periods of DJF, MAM and JJA. As shown in Fig. 5b, the correlation between the two data sets having absolute difference < 2 μg m^{-3} is highest in MAM (R ~ 0.76), followed by DJF (R ~ 0.73) and JJA (R ~ 0.61).

It has also been observed that absolute differences between the two data sets are smaller (Fig. 6) over the peninsular Indian locations where BC concentrations and seasonal variability are lower than the northern Indian locations (seasonal mean values of BC at each of locations are shown by the histograms). It is further evident from the figure that the absolute difference between BC_{SAT} and $BC_{SUR\text{-}N}$ significantly reduces at some of the locations of PI as compared to that between BC_{SAT} and BC_{SUR}; while the change in $BC_{SUR\text{-}N}$ from BC_{SUR} is not significant at several other locations. This indicates that the effect of boundary layer dynamics is different at different locations. During winter, even though the abundance of BC is confined near to the surface due to shallow PBL condition, the noon time PBL is much extended (close to or beyond 1-km) over most of the Indian locations (the spatio-temporal variability in PBL height is shown in supplementary Fig. S4). Thus, if the surface measured BC concentrations within the PBL are similar to the 1-km column average satellite retrieved BC, then $BC_{SUR\text{-}N}$ follows the same general trend as the original BC_{SUR}. During MAM and JJA, the PBL height is extended beyond 1-km at most of the Indian locations. Hence, comparing BC_{SAT} with $BC_{SUR\text{-}N}$ shows better agreement than that between BC_{SAT} and BC_{SUR}. Especially, the association between the two data sets significantly improves in JJA.

The northern part of India experiences significant seasonal changes in terms of incoming ground reaching solar radiation, with intense radiation during the pre-monsoon and monsoon months. This leads to significant seasonality in the PBL, that controls the vertical dispersion and hence the near surface loading (reduction) of aerosols. Based on air-borne in-situ measurements, Nair et al., (2016) have shown large seasonality (variation from winter to pre-monsoon) in the vertical profile of aerosol absorption coefficients over the IGP and Western India. Similarly, Brooks *et al.*, (2019) have reported nearly uniform distribution of BC through the vertical profile over NW India, IGP and the outflow region of IGP during monsoon.

Apart from seasonality, BC over the continental locations with low altitude above mean sea level show significant diurnal variability with day time low and night time high with a sharp peak after the sunrise. The increased convective activity during day time leads to deeper and more turbulent boundary layer and a faster dispersion of aerosols resulting in a decrease in concentration near the surface. Several recent studies have reported the prominent effect of PBL on the diurnal variability of BC, the amplitude of which vary significantly across the country, especially during winter (Babu et al., 2002; Beegum et al., 2009; Pathak et al., 2010; Gogoi et al., 2013, 2014; Kompalli et al., 2014; Prasad et al., 2018 etc.). In addition to the variability in atmospheric mixing and vertical dispersion of BC, accurate estimation of surface properties is another important parameter in the satellite retrieval. In particular, better estimates of surface properties during DJF and MAM could be the reason for improved correlations between satellite retrievals and surface BC concentrations, while the adverse atmospheric (clear, hazy or cloudy) and land surface (more wet soils) conditions might affect the ability to estimate fine mode aerosol concentrations during JJA.

https://doi.org/10.5194/acp-2022-555
Preprint. Discussion started: 19 September 2022

Atmospheric Chemistry and Physics Discussions

3.2 Soot Volume Fraction, SSA and BC Column Optical Depth

The soot volume fraction (*SVF*) or the volume fraction of BC in fine mode particles is an important parameter to understand the relative dominance of soot in the fine mode aerosol load in the column. Accurate estimate of SVF is essential for the quantification of the radiative effects of BC (Wang et al., 2016). In this study, an internal mixture of fine-mode aerosols is adapted to represent aerosol light absorption by SVF in the fine-mode particles. Thus, the representation of SVF should be regarded as an equivalent value, where the combination of various mixing states of aerosols (such as half internal and half external, core shell, and aggregated ones) are not considered in the retrieval (Hashimoto and Nakajima, 2017). The spatial distribution of the SVF at different months of winter, pre-monsoon, monsoon seasons (as shown in the supplementary Fig. S5) indicates that the ratio of soot in the entire aerosol mixture is as high as 5% over the IGP and northeastern parts of India. These values are similar to the mass fractions of BC reported by Gogoi et al., (2020) over the western, central and eastern part of the IGP based on air-borne in-situ measurements. The forgone observation thus suggests that the values of SVF estimated from the satellite-based observation is able to capture the broad regional features of columnar amounts of soot in fine mode particle concentrations. Based on sensitivity studies, Hashimoto and Nakajima (2017) have reported that the detection of an absorption by soot and dust particles is less uncertain over a high-reflecting surface and is spectrally more sensitive to the measurements of radiation at 380 nm of CAI-2 bands.

The monthly mean regional maps of SSA (at 546 nm) are shown in the Supplementary Fig. S6. The figure shows very large spatio-temporal variability, with values of SSA < 0.92 over most parts of the Indian region in December and January. In December, pockets of low SSA values (as low as 0.8) are observed over the western IGP, the Himalayan foothills, the NEI, and central India. The values of SSA over the IGP remains low until March and April, which also depict low values (~ 0.8) in its western part. It is evident from these observations that satellite-based retrieval of SSA from CAI-2 observations is capable of quantifying the spatio-temporal distribution of SSA, as found in several in-situ measurements. Based on in-situ vertical profiling of aerosol scattering and absorption properties on a research aircraft, Babu et al., (2016) have reported the values of SSA between 0.86 and 0.94 over different West Indian and IGP locations during the pre-monsoon (April-May) period. The values of SSA in our study are also in close agreement with those reported by Babu et al., (2016). Vaishya et al., (2018) have reported that there is a significant reduction in the SSA over the Himalayan foothills, the IGP regions and central India in pre-monsoon as compared to the winter season; while the peninsular India and adjoining oceanic regions show an increase. Just prior to the onset of monsoon, Vaishya et al., (2018) have also reported a decreasing gradient in SSA from the west to the east of IGP (~ 0.84 at west IGP, 0.73 at central IGP and 0.79 at eastern IGP; all at 530 nm). Over the oceanic regions, the values of SSA are, in general, high (> 0.95) and comparable to the surface values reported over the entire BoB (~ 0.93 during Mar-Apr) by Nair et al., (2008); Arabian sea (~ 0.9 in Mar) by Jayaraman et al., (2001).

Similar to SVF and SSA, significant regional and seasonal differencesin BC column optical depths (BC_{AOD}) are seen (Fig. 7) with values ranging from as low as 0.001 to as high as 0.1. During pre-monsoon months, BC_{AOD} over the IGP shows a gradual decline from Mar to May while the pattern is opposite over the NEI. BC_{AOD} shows pockets of high values over NEI in May. Increase in total columnar AOD over the IGP from Mar to May (peaks in Jun) is also reported by earlier investigators (Gautam et al., 2009; 2010) as against the opposite trend (peak in Mar) over the NEI (Pathak et al., 2016). The higher BC_{AOD} seen during Dec-Apr is indicative of the large amount of BC in the PBL during winter, both over the IGP (Singh et al., 2014; Vaishya et al., 2017) and NEI (Pathak et al., 2010; Guha et al., 2015) and its redistribution in the vertical column in the spring. This is further modulated by the occurance of seasonal fires over the Southeast Asia, which start appearing in December and increase in spatial extent and magnitude over time, to reach a peak duringMar/Apr/May (Sahu et al., 2021).

https://doi.org/10.5194/acp-2022-555
Preprint. Discussion started: 19 September 2022

Atmospheric Chemistry and Physics Discussions

3.3 Global distribution of BC from satellite retrievals

Considering fair association between the satellite retrieved and surface observations of BC over the Indian region, the global distribution is BC is examined at different months of winter, pre-monsoon and monsoon (Figs. 8, 9 and 10). Along with this, the global distribution of Fire Radiative Power (FRP in MW; shown in Supplementary Figures S7, S8 and S9) and the type of fire (presumed vegetation fire, active volcano, static land shore and offshore; shown in Supplementary Figures S10, S11 and S12) are also examined. In the present study, day time FRP with confidence level above 80% (high confidence; Giglio et al., 2020) is only used.

It is observed that the typical hot spots of BC prevailing throughout the year, though varying in magnitude, includes the biomass burning regions of South America, Africa, India and China. Enhanced values of BC are also seen in western Canada and USA, as well as over the Europe, Russia and part of China due to large fires occurring mainly in summer (JJA is marked by a large-scale outbreak of forest fires in the Russian Boreal Forests and South Africa; Justice et al., 1996; Wooster, 2004). The rainforest in Central Africa, being the largest biomass-burning region, shows large increase in the magnitude of BC during MAM and JJA. Amazon forest has lowest BC values during MAM. These observations clearly indicate that the spatio-temporal variability of BC across the globe is mostly coincident with the regions of intense biomass burning activities, while BC over some regions of south Asia and China do not collocate with the biomass burning regions. Interestingly, some oceanic regions near the coast of western Africa also show higher values of BC during DJF and JJA. Some offshore fires are also seen to be contributing to the BC load in the west coast of Africa. In line with our observations, Barkley et al., (2019) have reported the transport of African biomass burning aerosols to oceanic regions in the southern hemisphere. In another study based on GEOS-Chem-TOMAS global aerosol microphysics model simulations, Ramnarine et al., (2018) have reported the abundance of organic aerosols and BC in the remote areas of southern hemisphere downwind of biomass burning emissions from the Amazon in South America, the Congo in Africa, and some regions of the boreal forests in North America and Siberia.

The satellite-based observation of global BC distribution in the present study is also found to be in line with those reported by Bond et al., (2004), showing the major areas of BC emissions over north, central and South America, Europe, Russia, Middle East, Pacific, Africa, China and India. As reported in their study, significant BC emissions from forest fire activity over South America and Africa is clearly detected by the satellite-retrieved BC in our study, which peaks during DJF and JJA. Similarly, significant BC load seen over the regions of Russia during May-June period is coincident with the open burning areas, as reported by Bond et al., (2004). Several studies have reported that boreal forests and wild fires of Russia is crucial in the context of global carbon cycle, where large areas of Russian forest burn contribute to the net flux of carbon to the atmosphere.

4 Summary and Conclusions

This study investigates the regional and global distribution of BC based on satellite retrievals. Extensive measurements of near surface BC mass concentrations across a network of aerosol observatories (ARFINET) over the Indian region are used to evaluate and validate the spatio-temporal distribution of BC retrieved from Cloud and Aerosol Imager - 2 on-board Greenhouse gases Observing Satellite – 2. The main findings are as follows:

Regional distribution of BC from satellite retrieval (GOSAT-2 CAI-2) and surface measurements (ARFINET) during three distinct periods of December-January -February (DJF), March-April-May (MAM) and June-July-August (JJA) showed fairly good agreement between the two data sets over the Indian region. Especially during winter and pre-monsoon months, the satellite retrieval clearly identifies the regional hotspots of BC over India. The inter-comparison of satellite retrieved BC with the surface measurements revealed that for > 60% of the observations (for all the locations considered in this study) the absolute difference between the two data sets is < 2 µg m^{-3}. Associations between the two data sets having absolute difference < 2 µg m^{-3} is highest in MAM (R ~ 0.76), followed by DJF (R ~ 0.73) and JJA (R ~ 0.61).

https://doi.org/10.5194/acp-2022-555
Preprint. Discussion started: 19 September 2022


Atmospheric Chemistry and Physics Discussions

The spatial distribution of the soot volume fraction (SVF) at different months of winter, pre-monsoon, monsoon seasons is similar to that of the spatial distribution of BC over the Indian region with the ratio of soot in the entire aerosol mixture is > 5% over the IGP and northeastern parts of India. Regional distribution of aerosol single scattering albedo (SSA) shows values as low as 0.8 over the IGP and the northwestern part of India during winter and pre-monsoon season. Similar to SVF and SSA, significant regional and seasonal differences in BC column optical depths (BC_{AOD}) are seen with values ranging from as low as 0.001 to as high as 0.1. These observations are consistent with the data reported from in-situ measurements or other remote sensing platforms. All of these observations thus suggest the applicability of the CAI-2 aerosol products.

Most of the spatio-temporal variability of BC across the globe occurs with intensive biomass burning activities, except for some regions of south Asia and China. Enhanced values of BC are also seen in western Canada and USA, as well as over the Europe, Russia and part of China due to large fires occurring mainly in summer. Across South America, Africa, India, and China, BC is generally higher throughout the year, not just during times of biomass burning.

Data availability

Details of ARFINET ground-based data used in this manuscript and the point of contact are available at http://spl.gov.in; "Research Themes"; "Aerosols and Radiative Forcing". Information about satellite (GOSAT-2 CAI-2) data is available at https://www.gosat-2.nies.go.jp/about/data_products/.

Authors Contributions

This study was conceived by MMG and SSB in collaboration with RI and MH. Data processing and statistical analysis of the satellite and ground-based data were performed by MMG in consultation with SSB. All authors contributed to manuscript conceptualization, editing and review for submission. MMG drafted the initial manuscript with input from SSB. As far as ground-based aerosol data are concerned, MMG and SSB are responsible in the ARFINET; RI is the chief of the science team of the GOSAT-2 project; and MH is the developer of the inversion code. All authors read and approved the final manuscript.

Competing interests

The authors declare that they have no conflict of interest.

Acknowledgement

This work was carried out as part of the ARFI project of ISRO-GBP. This research work is also part of the joint agreement between ISRO and the sponsors of GOSAT-2 project: Japan Aerospace Exploration Agency (JAXA), the National Institute for Environmental Studies (NIES) and the Ministry of the Environment, Japan (MOE). MMG is the Principal Investigator of the Research Announcement on Greenhouse gases Observing SATellite Series (GOSAT RA). GOSAT-2/CAI-2 data are provided by JAXA/NIES/MOE. FRP (sftp://fuoco.geog.umd.edu) data is obtained from the Moderate resolution Imaging Spectroradiometer (MODIS). Global Monthly Fire Location Product (MCD14ML) is used for FRP. ERA-5 PBL data is obtained from ECMWF (https://apps.ecmwf.int/datasets/data/interim-full-daily/levtype=sfc/). The authors sincerely acknowledge Mr. Arun G.S. for his involvement in the processing of satellite and surface BC data.

https://doi.org/10.5194/acp-2022-555
Preprint. Discussion started: 19 September 2022

Atmospheric Chemistry and Physics Discussions

References

Babu, S. S. and Moorthy, K. K.: Aerosol black carbon over a tropical coastal station in India, Geophysical Research Letters, 29, 13-11-13-14, https://doi.org/10.1029/2002GL015662, 2002.

Babu, S. S., Manoj, M. R., Moorthy, K. K., Gogoi, M. M., Nair, V. S., Kompalli, S. K., Satheesh, S. K., Niranjan, K., Ramagopal, K., Bhuyan, P. K., and Singh, D.: Trends in aerosol optical depth over Indian region: Potential causes and impact indicators, Journal of Geophysical Research: Atmospheres, 118, 11,794-711,806, https://doi.org/10.1002/2013JD020507, 2013.

Babu, S. S., Nair, V. S., Gogoi, M. M. and Moorthy, K. K.: Seasonal variation of vertical distribution of aerosol single scattering albedo over Indian sub-continent: RAWEX aircraft observations, Atmospheric Environment, 125, 312-323, https://doi.org/10.1016/j.atmosenv.2015.09.041, 2016.

Bao, F., Cheng, T., Li, Y., Gu, X., Guo, H., Wu, Y., Wang, Y., and Gao, J.: Retrieval of black carbon aerosol surface concentration using satellite remote sensing observations, Remote Sensing of Environment, 226, 93-108, https://doi.org/10.1016/j.rse.2019.03.036, 2019.

Barkley, A. E., Prospero, J. M., Mahowald, N., Hamilton, D. S., Popendorf, K. J., Oehlert, A. M., Pourmand, A., Gatineau, A., Panechou-Pulcherie, K., Blackwelder, P., and Gaston, C. J.: African biomass burning is a substantial source of phosphorus deposition to the Amazon, Tropical Atlantic Ocean, and Southern Ocean, Proceedings of the National Academy of Sciences, 116, 16216-16221, https://doi.org/10.1073/pnas.1906091116, 2019.

Beegum, S. N., Moorthy, K. K., Babu, S. S., Satheesh, S. K., Vinoj, V., Badarinath, K. V. S., Safai, P. D., Devara, P. C. S., Sacchidanand, S., Vinod, Dumka, U. C., and Pant, P.: Spatial distribution of aerosol black carbon over India during pre-monsoon season, Atmospheric Environment, 43, 1071-1078, https://doi.org/10.1016/j.atmosenv.2008.11.042, 2009.

Bond, T. C., Doherty, S. J., Fahey, D. W., Forster, P. M., Berntsen, T., DeAngelo, B. J., Flanner, M. G., Ghan, S., Kärcher, B., Koch, D., Kinne, S., Kondo, Y., Quinn, P. K., Sarofim, M. C., Schultz, M. G., Schulz, M., Venkataraman, C., Zhang, H., Zhang, S., Bellouin, N., Guttikunda, S. K., Hopke, P. K., Jacobson, M. Z., Kaiser, J. W., Klimont, Z., Lohmann, U., Schwarz, J. P., Shindell, D., Storelvmo, T., Warren, S. G., and Zender, C. S.: Bounding the role of black carbon in the climate system: A scientific assessment, Journal of Geophysical Research: Atmospheres, 118, 5380-5552, https://doi.org/10.1002/jgrd.50171, 2013.

Bond, T. C., Streets, D. G., Yarber, K. F., Nelson, S. M., Woo, J.-H., and Klimont, Z.: A technology-based global inventory of black and organic carbon emissions from combustion, Journal of Geophysical Research: Atmospheres, 109, https://doi.org/10.1029/2003JD003697, 2004.

Brooks, J., Allan, J. D., Williams, P. I., Liu, D., Fox, C., Haywood, J., Langridge, J. M., Highwood, E. J., Kompalli, S. K., O'Sullivan, D., Babu, S. S., Satheesh, S. K., Turner, A. G., and Coe, H.: Vertical and horizontal distribution of submicron aerosol chemical composition and physical characteristics across northern India during pre-monsoon and monsoon seasons, Atmos. Chem. Phys., 19, 5615-5634, https://doi.org/10.5194/acp-19-5615-2019, 2019.

CAI-2 L2 Aerosol Retrieval ATBD, GOSAT-2/CAI-2 Level-2 aerosol retrieval Algorithm Theoretical Basis Document (ATBD), Under preparation.

CAI-2 L2 pre-processing ATBD, GOSAT-2 TANSO-CAI-2 L2 Pre-processing Algorithm Theoretical Basis Document (ATBD), NIES-GOSAT2-ALG-20191008-008-01, 2020.

https://doi.org/10.5194/acp-2022-555
Preprint. Discussion started: 19 September 2022

Atmospheric Chemistry and Physics Discussions

Choi, Y. and Ghim, Y. S.: Estimation of columnar concentrations of absorbing and scattering fine mode aerosol components using AERONET data, Journal of Geophysical Research: Atmospheres, 121, 13,628-613,640, https://doi.org/10.1002/2016JD025080, 2016.

Drinovec, L., Gregorič, A., Zotter, P., Wolf, R., Bruns, E. A., Prévôt, A. S. H., Petit, J. E., Favez, O., Sciare, J., Arnold, I. J., Chakrabarty, R. K., Moosmüller, H., Filep, A., and Močnik, G.: The filter-loading effect by ambient aerosols in filter absorption photometers depends on the coating of the sampled particles, Atmos. Meas. Tech., 10, https://doi.org/1043-1059, 10.5194/amt-10-1043-2017, 2017.

Dubovik, O., Herman, M., Holdak, A., Lapyonok, T., Tanré, D., Deuzé, J. L., Ducos, F., Sinyuk, A., and Lopatin, A.: Statistically optimized inversion algorithm for enhanced retrieval of aerosol properties from spectral multi-angle polarimetric satellite observations, Atmos. Meas. Tech., 4, 975-1018, https://doi.org/10.5194/amt-4-975-2011, 2011.

Dubovik, O., Lapyonok, T., Litvinov, P., Herman, M., Fuertes, D., Ducos, F., Lopatin, A., Chaikovsky, A., Torres, B., Derimian, Y., Huang, X., Aspetsberger, M., and Federspiel, C.: GRASP: a versatile algorithm for characterizing the atmosphere, SPIE Newsroom, https://doi.org/10.1117/2.1201408.005558, 2014.

Dubovik, O., Lapyonok, T., Litvinov, P., Herman, M., Fuertes, D., Ducos, F., Lopatin, A., Chaikovsky, A., Torres, B., Derimian, Y., Huang, X., Aspetsberger, M., and Federspiel, C.: GRASP: a versatile algorithm for characterizing the atmosphere, SPIE Newsroom, https://doi.org/10.1117/2.1201408.005558, 2014.

Fukuda, S., Nakajima, T., Takenaka, H., Higurashi, A., Kikuchi, N., Nakajima, T. Y., and Ishida, H.: New approaches to removing cloud shadows and evaluating the 380 nm surface reflectance for improved aerosol optical thickness retrievals from the GOSAT/TANSO-Cloud and Aerosol Imager, Journal of Geophysical Research: Atmospheres, 118, 13,520-513,531, https://doi.org/10.1002/2013JD020090, 2013.

Gautam, R., Hsu, N. C., and Lau, K.-M.: Premonsoon aerosol characterization and radiative effects over the Indo-Gangetic Plains: Implications for regional climate warming, Journal of Geophysical Research: Atmospheres, 115, https://doi.org/10.1029/2010JD013819, 2010.

Gautam, R., Hsu, N. C., Lau, K.-M., Tsay, S.-C., and Kafatos, M.: Enhanced pre-monsoon warming over the Himalayan-Gangetic region from 1979 to 2007, Geophysical Research Letters, 36, https://doi.org/10.1029/2009GL037641, 2009.

Giglio, L., Schroeder, W., Hall, J. V. and Justice, C. O.: MODIS Collection 6 Active Fire Product User's Guide, Revision C, NASA, 2020.

Gogoi, M. M., Babu, S. S., Moorthy, K. K., Bhuyan, P. K., Pathak, B., Subba, T., Chutia, L., Kundu, S. S., Bharali, C., Borgohain, A., Guha, A., De, B. K., Singh, B., and Chin, M.: Radiative effects of absorbing aerosols over northeastern India: Observations and model simulations, Journal of Geophysical Research: Atmospheres, 122, 1132-1157, https://doi.org/10.1002/2016JD025592, 2017.

Gogoi, M. M., Jayachandran, V. N., Vaishya, A., Babu, S. N. S., Satheesh, S. K., and Moorthy, K. K.: Airborne in situ measurements of aerosol size distributions and black carbon across the Indo-Gangetic Plain during SWAAMI–RAWEX, Atmos. Chem. Phys., 20, 8593-8610, https://doi.org/10.5194/acp-20-8593-2020, 2020.

Gogoi, M. M., Lakshmi, N. B., Nair, V. S., Kompalli, S. K., Moorthy, K. K., and Babu, S. S.: Seasonal contrast in the vertical profiles of aerosol number concentrations and size distributions over India: Implications from RAWEX aircraft campaign, Journal of Earth System Science, 128, 225, https://doi.org/10.1007/s12040-019-1246-y, 2019.

Gogoi, M. M., Moorthy, K. K., Sobhan Kumar, K., Jai Prakash, C., Babu, S. S., Manoj, M. R., Vijayakumar, S. N., and Tushar, P. P.: Physical and optical properties of aerosols in a free tropospheric environment: Results from long-term

https://doi.org/10.5194/acp-2022-555
Preprint. Discussion started: 19 September 2022

observations over western trans-Himalayas, Atmospheric Environment, 84, 262-274, https://doi.org/10.1016/j.atmosenv.2013.11.029, 2014.

Gogoi, M. M., S, K, Manoj, M. R., and Jai Prakash, C.: Absorption characteristics of aerosols over the northwestern region of India: Distinct seasonal signatures of biomass burning aerosols and mineral dust, Atmospheric Environment, 73, 92-102, https://doi.org/10.1016/j.atmosenv.2013.03.009, 2013.

Gogoi, M. M., Babu, S. S., Arun, B. S. et al.: Response of ambient BC concentration across the Indian region to the nation-wide lockdown: Results from the ARFINET measurements of ISRO-GBP, Current Science, 120, 2, 341-351, https://doi.org/10.18520/cs/v120/i2/341-351, 2021.

Guha, A., De, B. K., Dhar, P., Banik, T., Chakraborty, M., Roy, R., Choudhury, A., Gogoi, M. M., Babu, S. S., and Moorthy, K. K.: Seasonal Characteristics of Aerosol Black Carbon in Relation to Long Range Transport over Tripura in Northeast India, Aerosol and Air Quality Research, 15, 786-798, https://doi.org/10.4209/aaqr.2014.02.0029, 2015.

Gustafsson, Ö. and Ramanathan, V.: Convergence on climate warming by black carbon aerosols, Proceedings of the National Academy of Sciences, 113, 4243-4245, https://doi.org/10.1073/pnas.1603570113, 2016.

Hansen, A. D. A., Rosen, H., and Novakov, T.: The aethalometer — An instrument for the real-time measurement of optical absorption by aerosol particles, Science of The Total Environment, 36, 191-196, https://doi.org/10.1016/0048-9697(84)90265-1, 1984.

Hansen, A. D. A., Rosen, H., and Novakov, T.: The aethalometer — An instrument for the real-time measurement of optical absorption by aerosol particles, Science of The Total Environment, 36, 191-196, https://doi.org/10.1016/0048-9697(84)90265-1, 1984.

Hashimoto, M. and Nakajima, T.: Development of a remote sensing algorithm to retrieve atmospheric aerosol properties using multiwavelength and multipixel information, Journal of Geophysical Research: Atmospheres, 122, 6347-6378, https://doi.org/10.1002/2016JD025698, 2017.

Hsu, N. C., Jeong, M.-J., Bettenhausen, C., Sayer, A. M., Hansell, R., Seftor, C. S., Huang, J., and Tsay, S.-C.: Enhanced Deep Blue aerosol retrieval algorithm: The second generation, Journal of Geophysical Research: Atmospheres, 118, 9296-9315, https://doi.org/10.1002/jgrd.50712, 2013.

Hsu, N. C., Si-Chee, T., King, M. D., and Herman, J. R.: Aerosol properties over bright-reflecting source regions, IEEE Transactions on Geoscience and Remote Sensing, 42, 557-569, https://doi.org/10.1109/TGRS.2004.824067, 2004.

Hsu, N. C., Tsay, S., King, M. D., and Herman, J. R.: Deep Blue Retrievals of Asian Aerosol Properties During ACE-Asia, IEEE Transactions on Geoscience and Remote Sensing, 44, 3180-3195, https://doi.org/10.1109/TGRS.2006.879540, 2006.

IPCC, 2021: Climate Change 2021 - The Physical Science Basis. Contribution of Working Group I to the Sixth Assessment Report of the Intergovernmental Panel on Climate Change (Masson-Delmotte, V., P. Zhai, A. Pirani, S.L. Connors, C. Péan, S. Berger, N. Caud, Y. Chen, L. Goldfarb, M.I. Gomis, M. Huang, K. Leitzell, E. Lonnoy, J.B.R. Matthews, T.K. Maycock, T. Waterfield, O. Yelekçi, R. Yu, and B. Zhou (eds.)). Cambridge University Press, Cambridge, United Kingdom and New York, NY, USA, https://doi.org/10.1017/9781009157896.

Jayaraman, A., Satheesh, S. K., Mitra, A. P. and Ramanathan, V.: Latitude gradient in aerosol properties across the Inter Tropical Convergence Zone: Results from the joint Indo-US study onboard Sagar Kanya, Current Sci, 80, 10, 2001.

https://doi.org/10.5194/acp-2022-555
Preprint. Discussion started: 19 September 2022

Justice, C. O., Kendall, J. D., Dowty, P. R., and Scholes, R. J.: Satellite remote sensing of fires during the SAFARI campaign using NOAA Advanced Very High Resolution Radiometer data, Journal of Geophysical Research: Atmospheres, 101, 23851-23863, https://doi.org/10.1029/95JD00623, 1996.

Kaufman, Y. J.: Satellite sensing of aerosol absorption, Journal of Geophysical Research: Atmospheres, 92, 4307-4317, https://doi.org/10.1029/JD092iD04p04307, 1987.

Kompalli, S. K, K., Babu, S. S., Moorthy, K. K., Manoj, M. R., Kumar, N. V. P. K., Shaeb, K. H. B., and Ashok Kumar, J.: Aerosol black carbon characteristics over Central India: Temporal variation and its dependence on mixed layer height, Atmospheric Research, 147-148, 27-37, https://doi.org/10.1016/j.atmosres.2014.04.015, 2014.

Kondo, Y., Sahu, L., Kuwata, M., Miyazaki, Y., Takegawa, N., Moteki, N., Imaru, J., Han, S., Nakayama, T., Oanh, N. T. K., Hu, M., Kim, Y. J., and Kita, K.: Stabilization of the Mass Absorption Cross Section of Black Carbon for Filter-Based Absorption Photometry by the use of a Heated Inlet, Aerosol Science and Technology, 43, 741-756, https://doi.org/10.1080/02786820902889879,

Levy, R. C., Remer, L. A., Mattoo, S., Vermote, E. F., and Kaufman, Y. J.: Second-generation operational algorithm: Retrieval of aerosol properties over land from inversion of Moderate Resolution Imaging Spectroradiometer spectral reflectance, Journal of Geophysical Research: Atmospheres, 112, https://doi.org/10.1029/2006JD007811, 2007.

Lyapustin, A., Wang, Y., Laszlo, I., Kahn, R., Korkin, S., Remer, L., Levy, R., and Reid, J. S.: Multiangle implementation of atmospheric correction (MAIAC): 2. Aerosol algorithm, Journal of Geophysical Research: Atmospheres, 116, https://doi.org/10.1029/2010JD014986, 2011.

Manoj, M. R., Satheesh, S. K., Moorthy, K. K., Gogoi, M. M., and Babu, S. S.: Decreasing Trend in Black Carbon Aerosols Over the Indian Region, Geophysical Research Letters, 46, 2903-2910, https://doi.org/10.1029/2018GL081666, 2019.

Martins, J. V., Artaxo, P., Liousse, C., Reid, J. S., Hobbs, P. V., and Kaufman, Y. J.: Effects of black carbon content, particle size, and mixing on light absorption by aerosols from biomass burning in Brazil, Journal of Geophysical Research: Atmospheres, 103, 32041-32050, https://doi.org/10.1029/98JD02593, 1998.

Nair, V. S., Babu, S. S., Gogoi, M. M., and Moorthy, K. K.: Large-scale enhancement in aerosol absorption in the lower free troposphere over continental India during spring, Geophysical Research Letters, 43, 11,453-411,461, https://doi.org/10.1002/2016GL070669, 2016.

Nair, V. S., Moorthy, K. K., Alappattu, D. P., Kunhikrishnan, P. K., George, S., Nair, P. R., Babu, S. S., Abish, B., Satheesh, S. K., Tripathi, S. N., Niranjan, K., Madhavan, B. L., Srikant, V., Dutt, C. B. S., Badarinath, K. V. S., and Reddy, R. R.: Wintertime aerosol characteristics over the Indo-Gangetic Plain (IGP): Impacts of local boundary layer processes and long-range transport, Journal of Geophysical Research: Atmospheres, 112, https://doi.org/10.1029/2006JD008099, 2007.

Park, R. J., Minjoong, J. K., Jaein, I. J., Daeok, Y., and Sangwoo, K.: A contribution of brown carbon aerosol to the aerosol light absorption and its radiative forcing in East Asia, Atmospheric Environment, 44, 1414-1421, https://doi.org/10.1016/j.atmosenv.2010.01.042, 2010.

Pathak, B., Kalita, G., Bhuyan, K., Bhuyan, P. K., and Moorthy, K. K.: Aerosol temporal characteristics and its impact on shortwave radiative forcing at a location in the northeast of India, Journal of Geophysical Research: Atmospheres, 115, https://doi.org/10.1029/2009JD013462, 2010.

Pathak, B., Subba, T., Dahutia, P., Bhuyan, P. K., Moorthy, K. K., Gogoi, M. M., Babu, S. S., Chutia, L., Ajay, P., Biswas, J., Bharali, C., Borgohain, A., Dhar, P., Guha, A., De, B. K., Banik, T., Chakraborty, M., Kundu, S. S., Sudhakar, S., and

https://doi.org/10.5194/acp-2022-555
Preprint. Discussion started: 19 September 2022

Singh, S. B.: Aerosol characteristics in north-east India using ARFINET spectral optical depth measurements, Atmospheric Environment, 125, 461-473, https://doi.org/10.1016/j.atmosenv.2015.07.038, 2016.

Prasad, P., M, M, Wei-Nai, C., S, Mukunda, M. G., Sobhan Kumar, K., K, and S: Characterization of atmospheric Black Carbon over a semi-urban site of Southeast India: Local sources and long-range transport, Atmospheric Research, 213, 411-421, https://doi.org/10.1016/j.atmosres.2018.06.024, 2018.

Ramnarine, E., Kodros, J. K., Hodshire, A. L., Lonsdale, C. R., Alvarado, M. J., and Pierce, J. R.: Effects of near-source coagulation of biomass burning aerosols on global predictions of aerosol size distributions and implications for aerosol radiative effects, Atmos. Chem. Phys., 19, 6561-6577, https://doi.org/10.5194/acp-19-6561-2019, 2019.

Sahu, S. K., Mangaraj, P., Beig, G., Samal, A., Pradhan, C., Dash, S. and Tyagi, B.: Quantifying the high-resolution seasonal emission of air pollutants from crop residue burning in India, Environmental Pollution, 286, 117165, https://doi.org/10.1016/j.envpol.2021.117165, 2021.

Sand, M., Samset, B. H., Myhre, G., Gliß, J., Bauer, S. E., Bian, H., Chin, M., Checa-Garcia, R., Ginoux, P., Kipling, Z., Kirkevåg, A., Kokkola, H., Le Sager, P., Lund, M. T., Matsui, H., van Noije, T., Olivié, D. J. L., Remy, S., Schulz, M., Stier, P., Stjern, C. W., Takemura, T., Tsigaridis, K., Tsyro, S. G., and Watson-Parris, D.: Aerosol absorption in global models from AeroCom phase III, Atmos. Chem. Phys., 21, 15929-15947, https://doi.org/10.5194/acp-21-15929-2021, 2021.

Schuster, G. L., Dubovik, O., Holben, B. N., and Clothiaux, E. E.: Inferring black carbon content and specific absorption from Aerosol Robotic Network (AERONET) aerosol retrievals, Journal of Geophysical Research: Atmospheres, 110, https://doi.org/10.1029/2004JD004548, 2005.

Singh, A., Rajput, P., Sharma, D., Sarin, M. M., and Singh, D.: Black Carbon and Elemental Carbon from Postharvest Agricultural-Waste Burning Emissions in the Indo-Gangetic Plain, Advances in Meteorology, 2014, 179301, https://doi.org/10.1155/2014/179301, 2014.

Suresh Babu, S., S. Nair, V., M. Gogoi, M., and Krishna Moorthy, K.: Seasonal variation of vertical distribution of aerosol single scattering albedo over Indian sub-continent: RAWEX aircraft observations, Atmospheric Environment, 125, 312-323, https://doi.org/10.1016/j.atmosenv.2015.09.041, 2016.

Torres, O., Ahn, C., and Chen, Z.: Improvements to the OMI near-UV aerosol algorithm using A-train CALIOP and AIRS observations, Atmos. Meas. Tech., 6, 3257-3270, https://doi.org/10.5194/amt-6-3257-2013, 2013.

Torres, O., Bhartia, P. K., Herman, J. R., Ahmad, Z., and Gleason, J.: Derivation of aerosol properties from satellite measurements of backscattered ultraviolet radiation: Theoretical basis, Journal of Geophysical Research: Atmospheres, 103, 17099-17110, https://doi.org/10.1029/98JD00900, 1998.

Torres, O., Bhartia, P. K., Herman, J. R., Sinyuk, A., Ginoux, P., and Holben, B.: A Long-Term Record of Aerosol Optical Depth from TOMS Observations and Comparison to AERONET Measurements, Journal of the Atmospheric Sciences, 59, 398-413, 10.1175/1520-0469(2002)059<0398:Altroa>2.0.Co;2, 2002.

Torres, O., Tanskanen, A., Veihelmann, B., Ahn, C., Braak, R., Bhartia, P. K., Veefkind, P., and Levelt, P.: Aerosols and surface UV products from Ozone Monitoring Instrument observations: An overview, Journal of Geophysical Research: Atmospheres, 112, https://doi.org/10.1029/2007JD008809, 2007.

Vaishya, A, V., Prayagraj, S., Shantanu, R., and Babu, S. S.: Aerosol black carbon quantification in the central Indo-Gangetic Plain: Seasonal heterogeneity and source apportionment, Atmospheric Research, 185, 13-21, https://doi.org/10.1016/j.atmosres.2016.10.001, 2017.

https://doi.org/10.5194/acp-2022-555
Preprint. Discussion started: 19 September 2022

Atmospheric Chemistry and Physics Discussions

Vaishya, A., Babu, S. N. S., Jayachandran, V., Gogoi, M. M., Lakshmi, N. B., Moorthy, K. K., and Satheesh, S. K.: Large contrast in the vertical distribution of aerosol optical properties and radiative effects across the Indo-Gangetic Plain during the SWAAMI–RAWEX campaign, Atmos. Chem. Phys., 18, 17669-17685, 10.5194/acp-18-17669-2018, 2018.

Vignati, E., Karl, M., Krol, M., Wilson, J., Stier, P., and Cavalli, F.: Sources of uncertainties in modelling black carbon at the global scale, Atmos. Chem. Phys., 10, 2595-2611, 10.5194/acp-10-2595-2010, 2010.

Wang, L., Li, Z., Tian, Q., Ma, Y., Zhang, F., Zhang, Y., Li, D., Li, K., and Li, L.: Estimate of aerosol absorbing components of black carbon, brown carbon, and dust from ground-based remote sensing data of sun-sky radiometers, Journal of Geophysical Research: Atmospheres, 118, 6534-6543, https://doi.org/10.1002/jgrd.50356, 2013.

Wang, R., Balkanski, Y., Boucher, O., Ciais, P., Schuster, G. L., Chevallier, F., Samset, B. H., Liu, J., Piao, S., Valari, M., and Tao, S.: Estimation of global black carbon direct radiative forcing and its uncertainty constrained by observations, Journal of Geophysical Research: Atmospheres, 121, 5948-5971, https://doi.org/10.1002/2015JD024326, 2016.

Wooster, M. J. and Zhang, Y. H.: Boreal Forest fires burn less intensely in Russia than in North America, Geophysical Research Letters, 31, https://doi.org/10.1029/2004GL020805, 2004.

https://doi.org/10.5194/acp-2022-555
Preprint. Discussion started: 19 September 2022

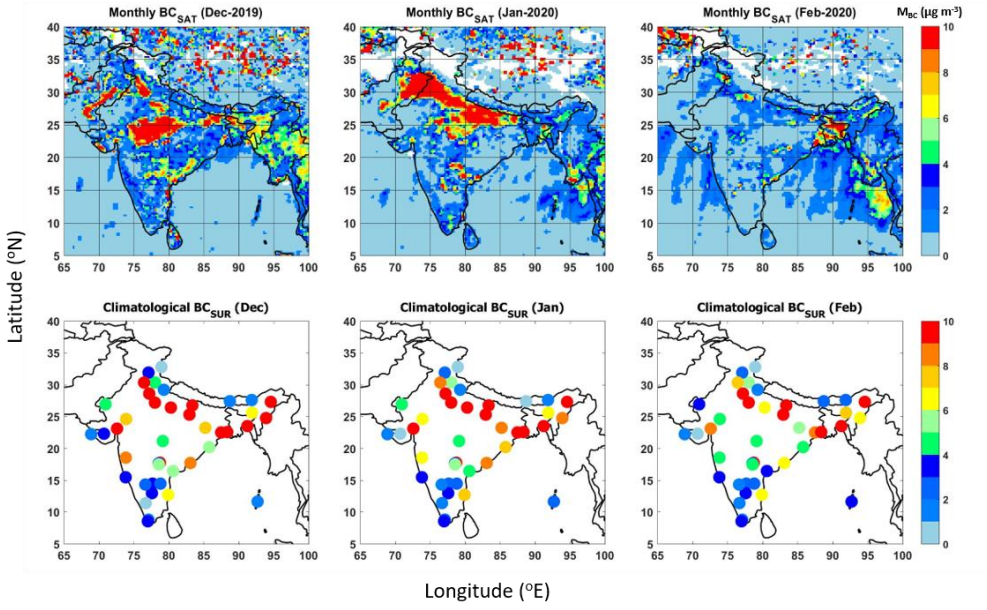

Figure 1: Regional distribution of monthly average BC over the Indian region from satellite (of the year 2019-2020) and surface measurements (climatological monthly average) during Dec-Jan-Feb (DJF) representing winter. The satellite-retrieved BC values (BC_{SAT}) are shown at 0.25 x 0.25 degrees spatial resolution. The surface BC (BC_{SUR}) in the bottom panel are climatological monthly average values at the point locations of the ARFINET. Minimum 3 to more than 10 years of data are included for the estimation of the climatological average. The color bars indicate the magnitudes of monthly average BC mass concentrations.

https://doi.org/10.5194/acp-2022-555
Preprint. Discussion started: 19 September 2022

Atmospheric Chemistry and Physics Discussions

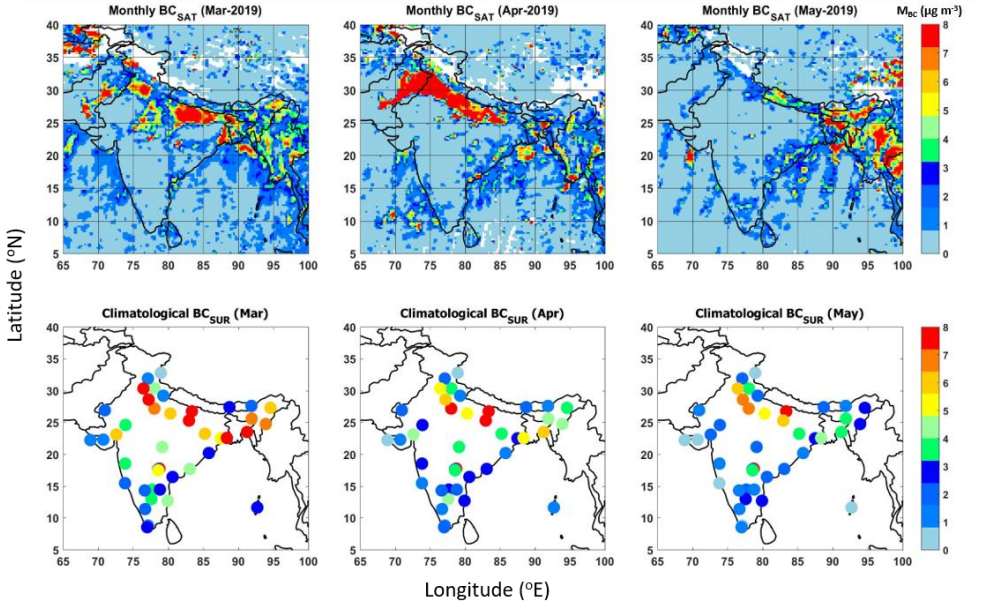

605

Figure 2: Same as Figure-1, for Mar-Apr-May (MAM), representing the pre-monsoon.

https://doi.org/10.5194/acp-2022-555
Preprint. Discussion started: 19 September 2022

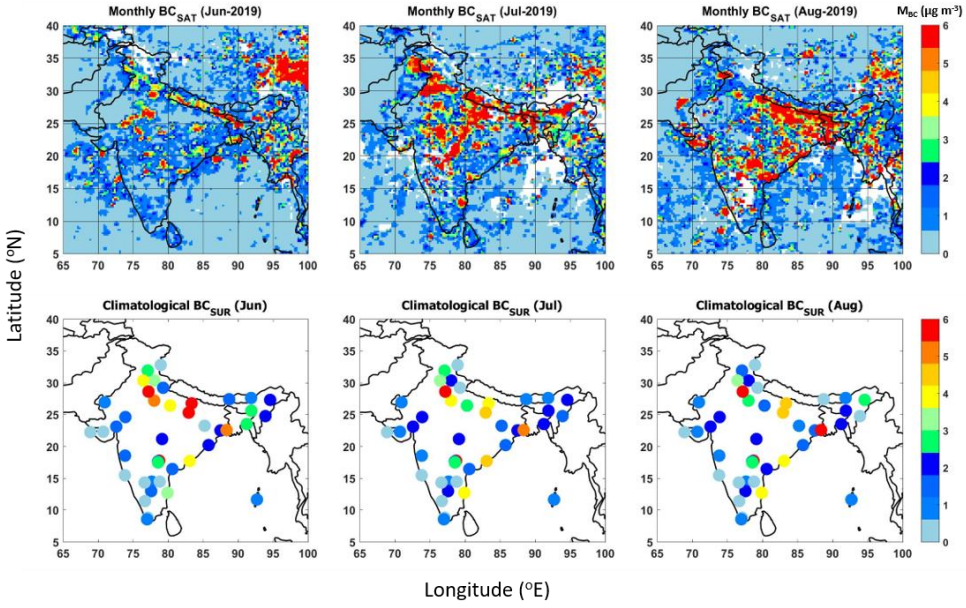

Figure 3: Same as Fig.1 and Fig.2 above, for Jun-Jul-Aug (JJA) representing monsoon.

610

https://doi.org/10.5194/acp-2022-555
Preprint. Discussion started: 19 September 2022

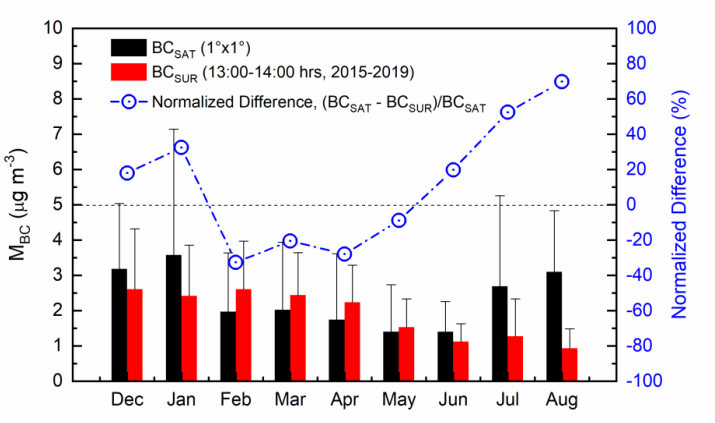

Figure 4: Monthly variation of the regional average values (averaged over all the locations considered for inter-comparison) of BC concentrations from satellite retrievals (BC_{SAT}) and surface measurements (BC_{SUR}), along with the normalized difference (in %) between the two data sets.

615

https://doi.org/10.5194/acp-2022-555
Preprint. Discussion started: 19 September 2022

Atmospheric Chemistry and Physics Discussions

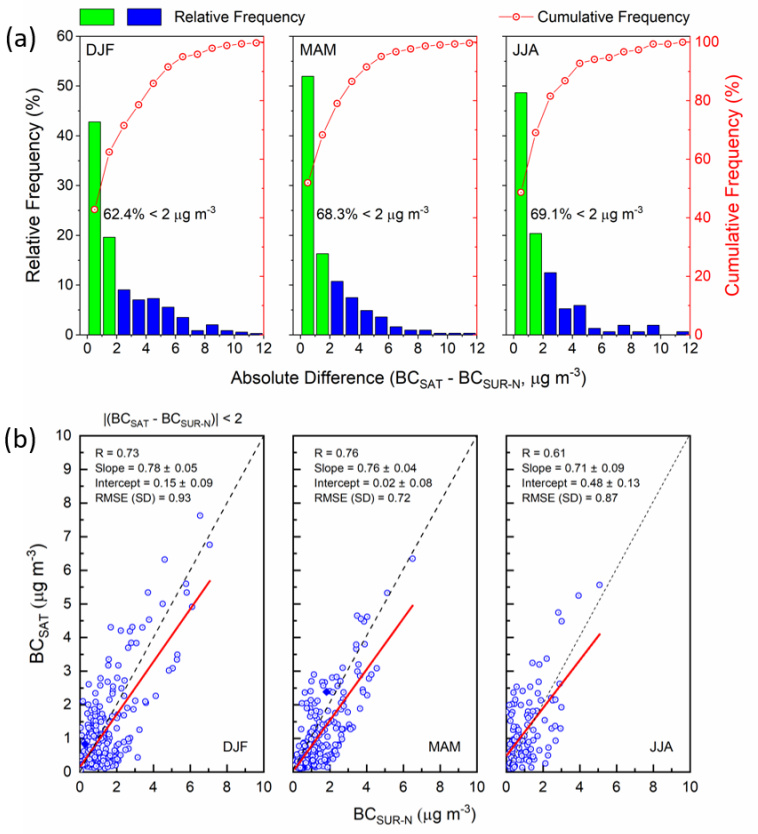

Figure 5: (a) Frequency counts (in percentage) of the absolute difference in BC (in μg m^{-3}) between simultaneous satellite (BC_{SAT}, averaged over 1 x 1-degree area around each of the ARFINET sites) and normalized surface BC (BC_{SUR-N}) concentrations; (b) Association between simultaneous satellite and normalized surface BC concentration. The solid red line is the linear fit, and the grey dash line is the one-to-one line of BC_{SAT} and BC_{SUR-N}.

https://doi.org/10.5194/acp-2022-555
Preprint. Discussion started: 19 September 2022

Atmospheric Chemistry and Physics Discussions

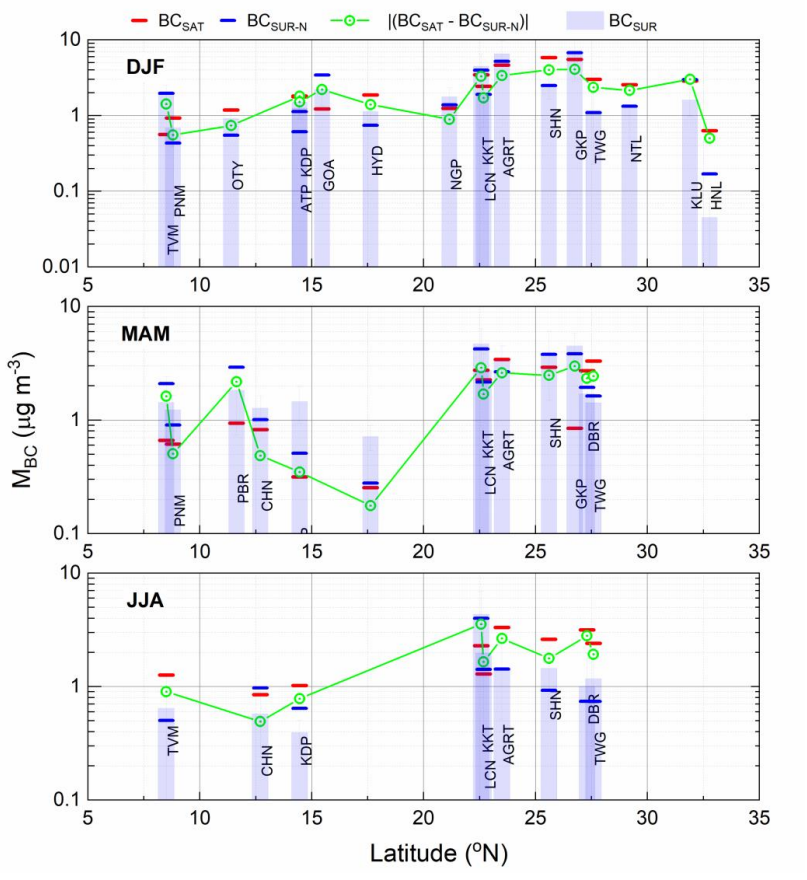

635

Figure 6: Seasonal mean values of satellite-retrieved (BC_{SAT}) and surface BC (BC_{SUR} and $BC_{SUR\text{-}N}$) concentrations, along with the absolute difference between BC_{SAT} and $BC_{SUR\text{-}N}$ at different locations during DJF (top), MAM (middle) and JJA (bottom). Locations are arranged by latitudes. Also shown are names of individual stations (details in supplementary Table-T1).

640

645

650

https://doi.org/10.5194/acp-2022-555
Preprint. Discussion started: 19 September 2022

Atmospheric Chemistry and Physics Discussions

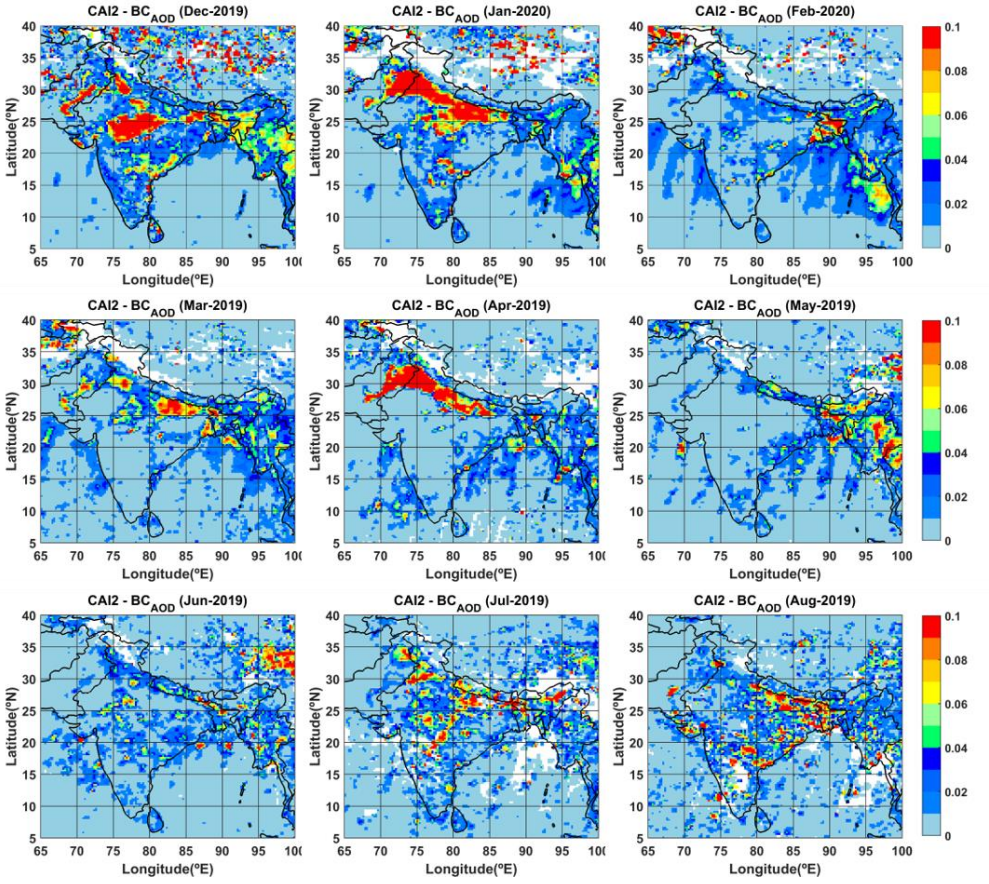

Figure 7: Regional distribution (0.25 x 0.25 degree) of monthly mean BC column optical depth (BC_{AOD}) over India during DJF, MAM and JJA of the years 2019-2020.

655

660

665

670

https://doi.org/10.5194/acp-2022-555
Preprint. Discussion started: 19 September 2022

Atmospheric Chemistry and Physics Discussions

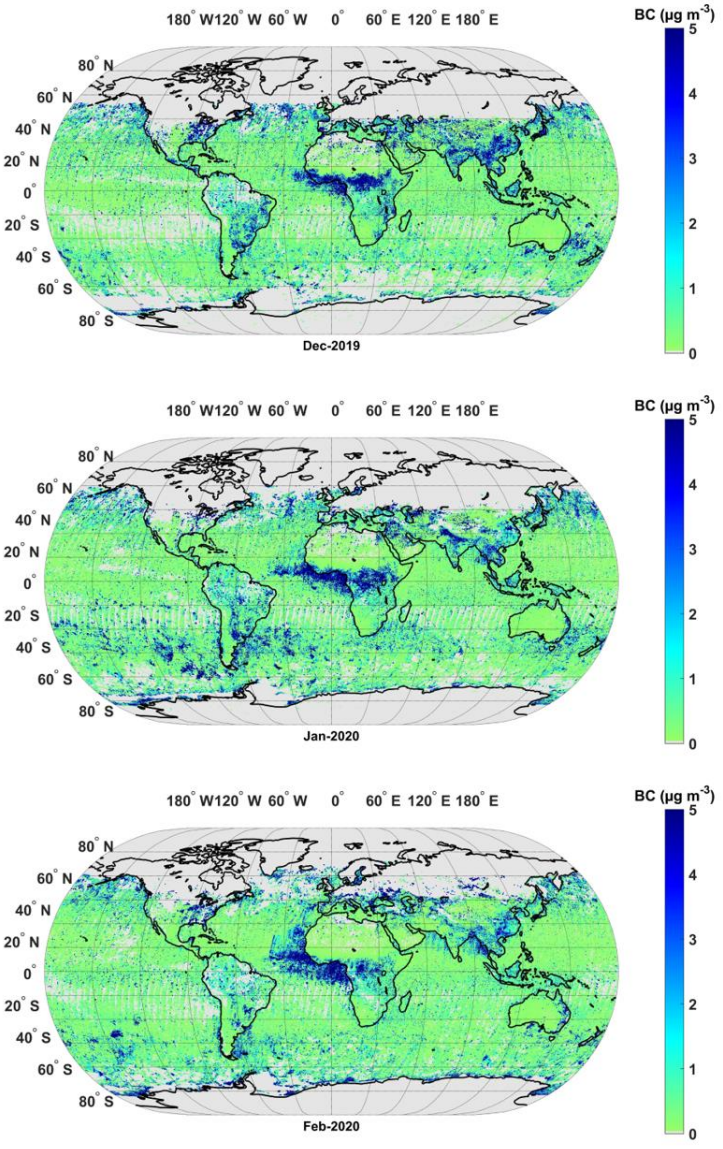

Figure 8: Global map of satellite retrieved BC (0.25 x 0.25 degree) during DJF.

https://doi.org/10.5194/acp-2022-555
Preprint. Discussion started: 19 September 2022

Atmospheric Chemistry and Physics Discussions

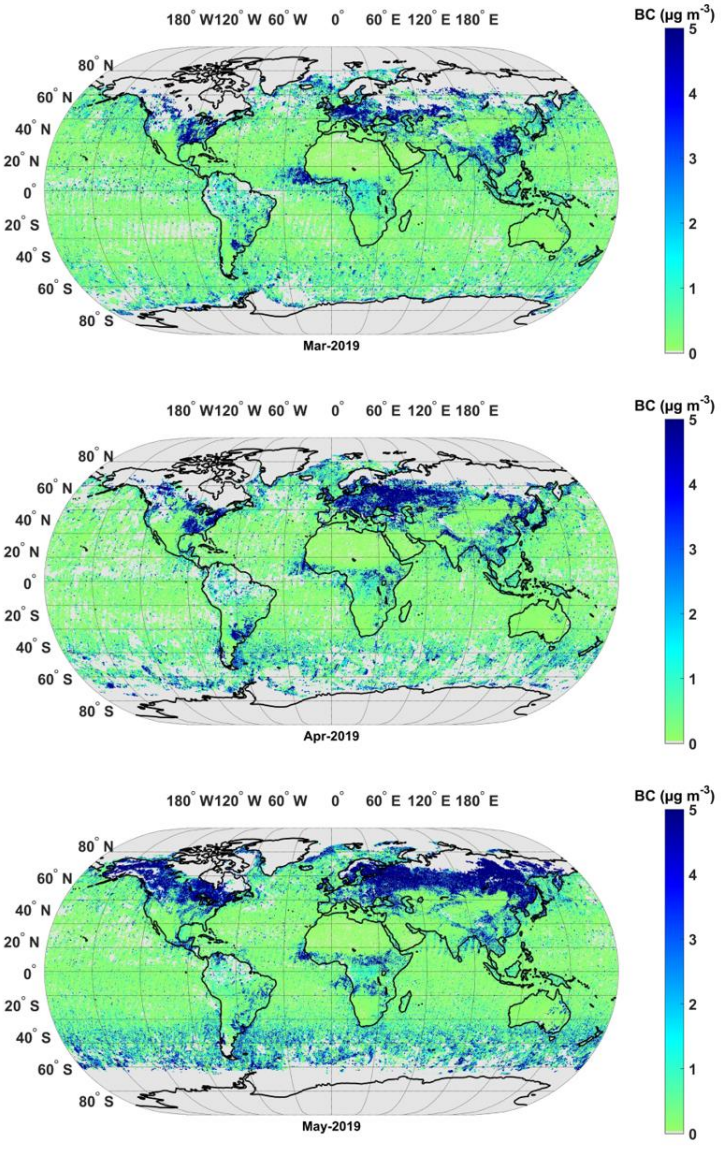

675

Figure 9: Global map of satellite retrieved BC (0.25 x 0.25 degree) during MAM.

https://doi.org/10.5194/acp-2022-555
Preprint. Discussion started: 19 September 2022

Atmospheric Chemistry and Physics Discussions

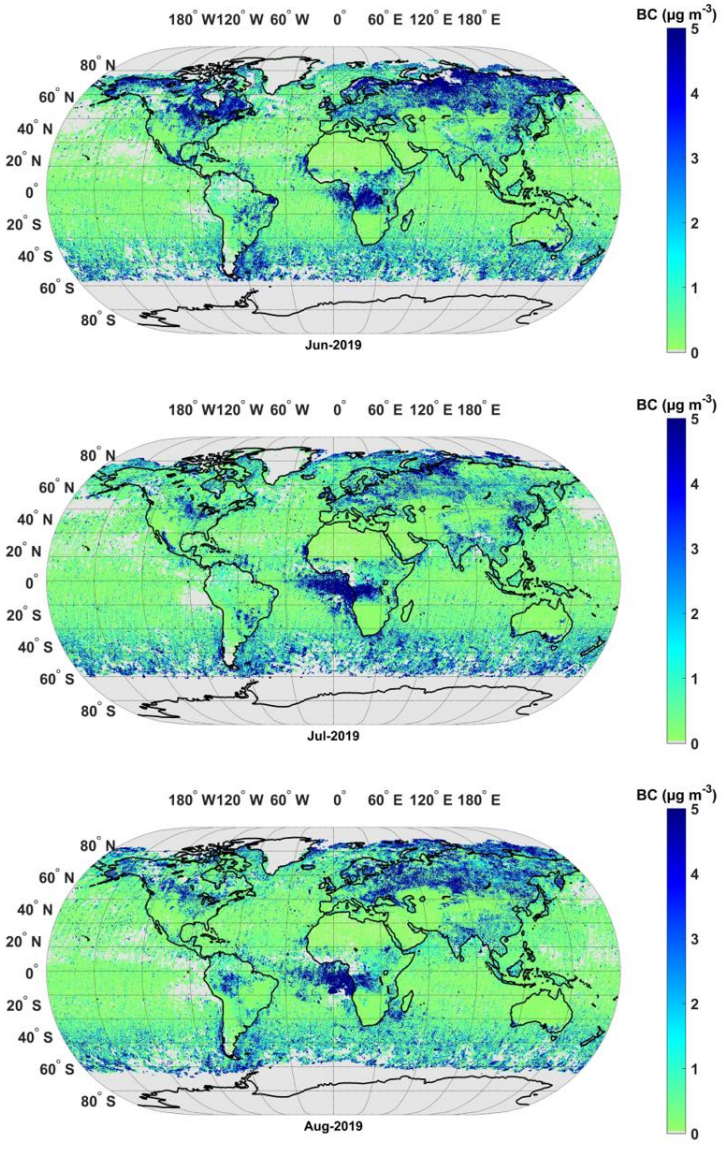

680 **Figure 10: Global map of satellite retrieved BC (0.25 x 0.25 degree) during JJA.**

https://doi.org/10.5194/acp-2022-555
Preprint. Discussion started: 19 September 2022

Atmospheric Chemistry and Physics Discussions

685 **Table 1: Regional average BC over India from satellite and surface measurements. The satellite-based estimate is made from 1 x 1 degree area average values around each of the ARFINET sites; while the climatological surface BC is for the period from 2015-2019 (13:00 to 14:00 hrs. local time).**

Period	Average BC over India (μg m^{-3})		
	BC_{SAT}	BC_{SUR}	Normalized Difference (%)
DJF	2.91 ± 0.84	2.54 ± 0.11	12.7
MAM	1.72 ± 0.31	2.06 ± 0.47	-19.7
JJA	2.39 ± 0.89	1.11 ± 0.17	53.5